RSC Advances

ROYAL SOCIETY OF CHEMISTRY

www.rsc.org/advances

RCS Advances

RSCPublishing

ARTICLE

Transparent nanophosphor films with high quantum efficiency through cold compaction

Cite this: DOI: 10.1039/x0xx00000x

R. Kubrin,[ab] J. J. do Rosario[a] and G. A. Schneider[a] ,

Received 00th January 2012,
Accepted 00th January 2012

DOI: 10.1039/x0xx00000x

www.rsc.org/

A facile method to improve transparency, mechanical stability and quantum yield (QY) of luminescent nanoparticle films is presented. Porous layers of crystalline Y_2O_3:Eu nanophosphor with an average particle size of 24 nm were produced by flame spray pyrolysis. The coatings were sandwiched between two rigid substrates and exposed to cold isostatic pressing (CIP) at 900 MPa. The second substrate could be removed afterwards without damage. Compaction increased the particle packing density up to 60 vol.% and nearly eliminated light scattering in the films, thus making them transparent throughout the visible range. At the same time, the luminescence decay time constant decreased from 3.3 to 1.4 ms confirming an increase of internal QY of the nanophosphor from 0.31 to 0.60. A good match of experimental data with nanocrystal cavity model of radiative decay of photoluminescence was demonstrated. The increase of external brightness of the coatings was limited to 28 % (for thin coatings it even decreased) due to the onset of light trapping by multiple internal reflection. Deliberate introduction of scatterers on the surface of the film allowed increasing the extracted intensity by at least 70 %, thus reaching 55 % of the maximum brightness of a commercial micrometer-sized Y_2O_3:Eu phosphor powder. The CIP-processed coatings possessing final thickness between 1 and 12 µm behaved as smooth crack-free solid films with excellent mechanical stability. The proposed method of cold compaction offers an advantage of rapid processing avoiding high-temperature post-treatment for all applications of transparent phosphor films and other optical coatings.

Introduction

One of the most important general assets of luminescent nanoparticles is their vanishingly small light scattering efficiency, which makes them particularly attractive for applications demanding high optical transparency: transparent plasma display devices,[1] phosphor-converted white light-emitting diodes (LEDs),[2] and radiation converters for dye-sensitized solar cells.[3] Fabrication of transparent luminescent ceramics usually requires sintering of pre-shaped powder samples at high temperatures followed by polishing of the surfaces. Calcination- and sintering-free deposition of transparent nanophosphor films has been studied by numerous research groups.[1,2,4-10] All published methods are based on multi-step wet processing and often involve addition of polymers as host materials. Alternatively, phosphor nanoparticles could be continuously produced and coated onto substrates by flame aerosol deposition (FAD),[11] a rapid single-step processing method based on flame spray pyrolysis (FSP).[12] FAD results in homogeneous nanoparticulate films from liquid solutions within minutes and is successfully applied for deposition of optical fiber preforms,[13] gas sensors,[14] anti-fogging films,[15] dye-sensitized solar cells,[16] microfluidic devices,[17] and flexible multifunctional nanocomposite films.[18] The main drawback of FAD is that it usually produces deposits with very low packing density of nanoparticles (corresponding to volumetric porosity on the order of 98 %)[14] and poor mechanical properties. In most applications denser, more stable coatings are desired. In the case of a luminescent material, the nanoparticle volume fraction directly affects the brightness of emission and scattering losses of the light transmitted through the film.[11] Having the means to increase the packing density would be clearly beneficial for the performance of nanophosphor screens in terms of quantum efficiency, transparency, and screen resolution (for imaging applications[19]).

Cold compaction of non-luminescent TiO_2 nanoparticle films has been developed for fabrication of photoelectrodes for the flexible dye-sensitized solar cells (DSSC).[20-24] Mechanical compression of titanium dioxide films deposited by FAD was also implemented recently by means of low pressure lamination.[25] One of the general challenges encountered in compaction of flexible photoelectrodes of DSSCs, which usually have a thickness on the order of 10 µm, is the uniformity of applied pressure over the area as it requires special care in adjustment

of parallelism and flatness of the pressing platens or rolls. To improve on this issue, application of cold isostatic pressing (CIP) was suggested.[26] It has been shown that CIP-compaction increases the scratch resistance of the TiO_2 films [27] and also substantially improves their transparency.[28]

It is known that a change of particle packing density has a strong influence on light scattering and radiative emission decay rate of luminescent nanoparticles.[11] To the best of our knowledge, the effect of compaction on optical properties of nanoparticulate films has not been systematically studied and application of compaction techniques to nanophosphor coatings has never been reported.

In the present work, an attempt to radically compact FAD deposits is undertaken. We deploy high-pressure CIP to compress Y_2O_3:Eu nanophosphor coatings sandwiched between two rigid substrates (thus, effectively applying the force uniaxially). Optical transparency, photoluminescent (PL-) performance and mechanical properties of compacted coatings are investigated. The chemical composition of the nanophosphor was previously optimized for the best performance.[11] We show that by FAD and mechanical compaction it is possible to obtain mechanically stable transparent nanophosphor coatings within several minutes without any thermal post-processing.

Experimental

Deposition of coatings: The deposition of Y_2O_3:Eu nanophosphor coatings performed at the Particle Technology Laboratory at the Swiss Federal Institute of Technology (Zurich, Switzerland) was thoroughly described in our previous work.[11] Hydrates of yttrium nitrate (99.9 %, ChemPur) and europium nitrate (99.9 %, Alfa Aesar) were dissolved in ethanol (EtOH, p.a.) and 2-ethylhexanoic acid (EHA, 99 %, Riedel-de Haën), so that a 0.5 M solution of yttrium and europium nitrates in a solvent composed of 50 vol.% EtOH and 50 vol.% EHA was obtained. The flammable liquid precursor was fed into the flame with a syringe pump at the rate of 11.7 ml min^{-1} through a capillary of an outside-mixing two-phase nozzle. The precursor was dispersed with oxygen (at the rate of 3 l min^{-1}, with a constant pressure drop of 1.5 bar over the nozzle). The liquid spray was ignited with a methane/oxygen pilot flame (1.4 and 2.8 l min^{-1}, respectively). Samples of the phosphor doped 8 mol.% europium with coating densities up to 4 mg cm^{-2} were produced on water-cooled fused quartz substrates (30 mm diameter, 1 mm thick, double-side polished) placed in 25 cm above the burner nozzle. The average particle size derived from the measurements of specific surface area was 24 nm and the crystalline structure was mainly cubic (containing 15-18 wt.% of the monoclinic phase).[11] As a reference, a coating deposited by gravitational sedimentation of a commercial phase-pure cubic Y_2O_3:Eu phosphor (MaTecK GmbH, 4.5 % Eu, d_{SEM} = 4 μm, coating density 2.0 mg cm^{-2}) was used.[29]

Compaction: To mechanically compact the FAD deposits, a blank fused quartz substrate was put on the coated side of each sample, thus "sandwiching" the nanoparticle layer between the quartz plates. The two substrates were gently pressed together (manually) until the blank one sufficiently adhered to the sample to allow further handling. The "sandwich" was enclosed in an elastic air-tight casing and introduced in the cold isostatic press (KIPP200ES, Paul Weber, Remshalden-Brunbach, Germany). The samples were compressed at a pressure of 900 MPa for 2 min. Pressurizing and depressurizing steps also had a duration of 2 min. The substrates could be later separated by introducing a scalpel blade between them. The compacted FAD coating always stayed on its original substrate.

Characterization: The morphology of deposited layers was investigated by scanning electron microscopy (SEM: LEO 1530 Gemini). The porosity of the coatings was calculated from their apparent thickness (obtained from SEM of cleaved samples) and coating density (obtained by weighing the substrates before and after FAD). Measurements of hardness and elastic modulus of compressed coatings were performed with a Nano Indenter G200 system (Agilent Technologies, USA) equipped with a standard XP indenter head with the Berkowich geometry. The constant stiffness measurement (CSM) technique and an indentation depth of 5 μm were used. The measurements were performed on the thickest sample (12 μm) in order to minimize the error due to proximity of the substrate. Indents were distributed over the sample surface. Attenuance spectra of the FAD coatings were taken with a Perkin Elmer "Lambda 1050" and a Varian "Cary 500" UV-Vis-NIR spectrometers. The photoluminescence of the nanophosphor powders was examined with a Varian Cary Eclipse fluorescence spectrometer. The measurements of the PL-emission spectra were performed by exciting the phosphor with a Xe flash lamp at a wavelength of 254 nm. The brightness of photoluminescence of the phosphor coatings was measured by a portable photospectrometer (Tristan 4, MUT GmbH). A low-pressure mercury lamp (NU-8 KL, Konrad Benda) at the wavelength of 254 nm was used as an excitation source. Screen brightness was determined by the amplitude of the main emission peak (λ = 612 nm). Thickness of all samples except the thinnest one (0.23 mg cm^{-2}) was sufficient to absorb most of the incident UV-light so that in most cases the intensity of emission did not depend on exact value of coating density.[11]

Results and discussion

Packing density of nanoparticles and mechanical properties of the coatings

Standard FAD technique implemented for yttria-based nanophosphors resulted in deposits with very sparsely packed nanoparticles (Figure 1a) corresponding to a particle volume fraction of only 2.7±0.4 % (97.3 vol.% porosity).[11] After compaction of films with a coating weight of 3.8 mg cm^{-2} at 900 MPa, the particle volume fraction estimated from the cross-sectional SEM (Figure 1b) reached 59.6±1.5 %, thus approaching the upper limits of loose random packing of monosized spherical particles.[30] In Figure 1 c) and d), high-magnification views of

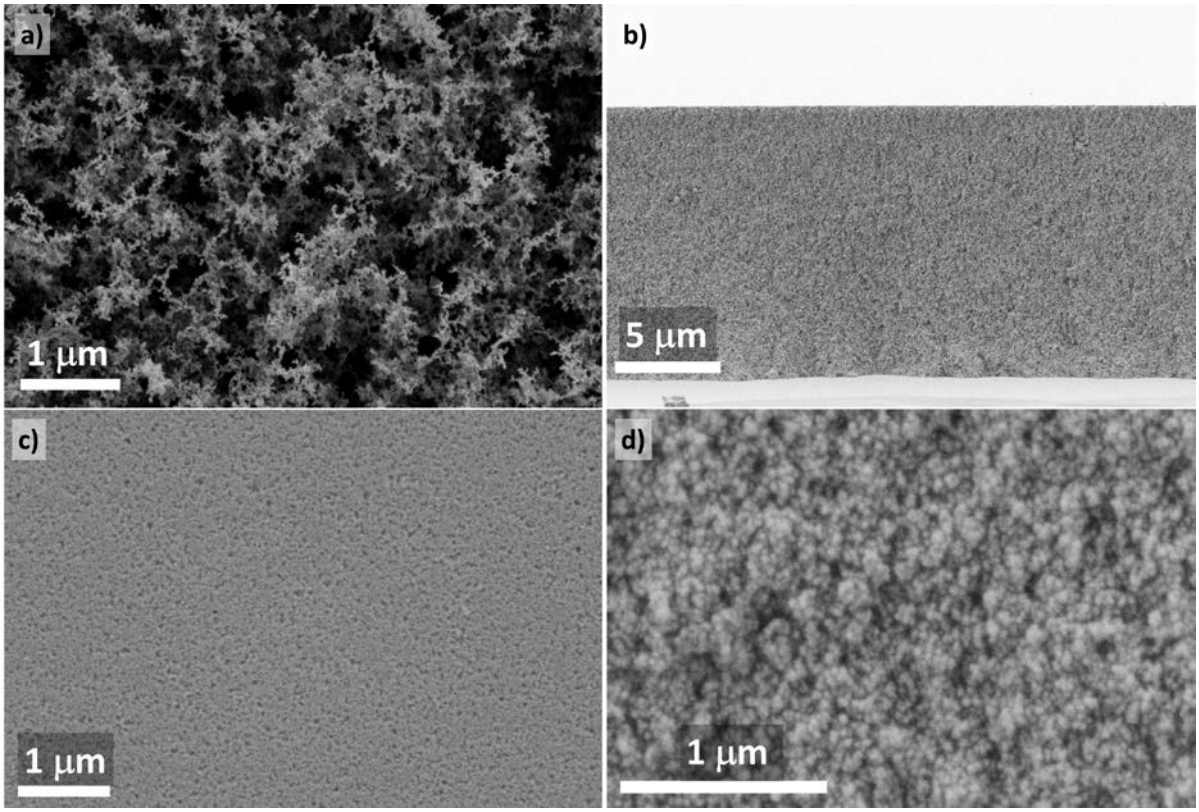

Figure 1. a) SEM of an as-deposited Y_2O_3:Eu nanophosphor coating (top surface); b) cross-section of a compacted sample; c) top surface of a compacted layer; d) fracture surface of a compacted layer.

the top surface and fracture surface are shown, respectively. Compressed coatings featured no cracks at the cm-scale and surface roughness was on the order of the size of several nanoparticles.

More than 20-fold densification of the nanophosphor coatings could be anticipated to dramatically affect their mechanical properties. In the initial state (before compaction), no data could be obtained with the available equipment because the event of contact between the indenter tip and the coating could not be detected. Figure 2 shows the results of nanoindentation performed on CIP-processed coatings. Load-displacement curves (Figure 2a) show a typical indentation profile with a continuous loading curve followed by holding and unloading segments. The absence of discontinuities in the load-displacement curves indicates homogeneity of the layer. Starting from the indentation depth of about 1000 nm, the film hardness was on the order of 1.5-1.6 GPa (Figure 2b). The curves of elastic modulus revealed a reproducible increase from approximately 50 GPa at the depth of 1000 nm to about 60 GPa at 4000 nm (Figure 2c), which should be attributed to film densification as the indenter tip penetrates deeper into it.

When compared to the literature on mechanical performance of transparent yttria (hardness 10.7 GPa, elastic modulus 178-185 GPa),[31] the properties of the nanophosphor coatings are surely significantly worse than those of the fully sintered material. Nevertheless, this performance should constitute a sufficient mechanical stability for many applications. As opposed to the original FAD coatings, compressed deposits could not be destroyed by touching their surface and a tool was needed to scratch them off the substrate. A successful substrate transfer of compacted FAD-produced TiO_2 film possessing the elastic modulus below 2 MPa was demonstrated.[25] Furthermore, it can be expected that the particle volume fraction and mechanical properties of the nanophosphor coatings could be tuned between the original state and the values achieved in the present work by simply varying the applied pressure.[20]

The thinnest compacted coating had a coating density of 0.23 mg cm^{-2}. Its geometrical thickness in the initial state was approximately 16 μm. Nevertheless, even such a thin layer retained its integrity upon "sandwich"-compaction and removal of the second substrate. The thickness in the compacted state was 1.0±0.1 μm, which corresponds to 43.4±4.4 vol.% particle fraction, substantially lower than that of the thick coatings. Worse compaction could be related to the small coating thickness representing a challenge for the planarity of the substrates. Processing of the films with thickness below 1 μm would obviously require special care for the choice of the substrates.

The films of intermediate coating density (1.2 mg cm^{-2}) could be compressed to a thickness of at least 4.2 μm, which corresponds to a particle fraction of 55.0±1.5 vol.%.

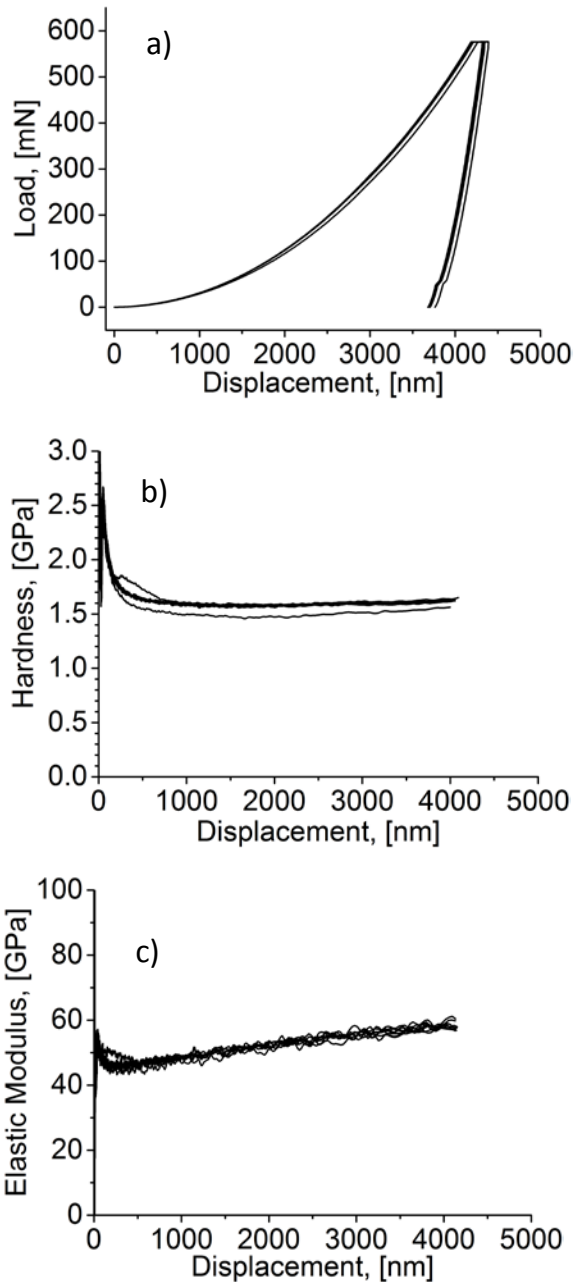

Figure 2. a) Load-displacement curves from nanoindentation; b) hardness-displacement curves; c) Elastic modulus-displacement curves.

Optical transparency of the nanophosphor films

The remarkable changes in the optical properties of the nanophosphor coatings could be observed by naked eye (Figure 3). When compared to the conventional phosphor coatings consisting of micrometer- or submicrometer-sized particles with the equal coating density, as-deposited FAD-coatings had up to two orders of magnitude lower scatterance in the visible range.[11] Nevertheless, at the high coating densities of approximately 4 mg cm^{-2}, even the nanophosphor films became rather translucent (Figure 3a) so that the incident light experienced multiple scattering before escaping from the coating. The values of attenuance (expressing the losses due to absorption and scattering) measured for such thick coatings in the visible range were quickly growing from 0.8 (~15 % transmittance) at the wavelength of 800 nm to 2.7 around 380 nm (< 0.2 % transmittance, Figure 4a); the rest of the incident light was scattered in all directions. We assume here that absorption of visible light can be neglected for our films so that the attenuance equals the scatterance.

Figure 3b shows that the compressed coatings were fully transparent. Practically no blur of images in the background was observed. Attenuance shifted well below 0.5 throughout the visible range. For example, for the main emission wavelength of the Y_2O_3:Eu phosphor (612 nm), it was equal to 0.146 units, which means that at least 71 % of the incident photons would be transmitted through the coating without being scattered or reflected. Some residual scattering was surely still present because the transmission losses on the order of 29 % could not be explained exclusively by the Fresnel reflection loss. The effective refractive index of the compacted nanophosphor n_{EFF} can be estimated by the linear permittivity mixing rule

$$n_{EFF} = \sqrt{f_V n_P^2 + (1 - f_V)} \quad (1)$$

where f_V is the particle volume fraction and n_P is the refractive index of the dense bulk phosphor. Taking the refractive index of Y_2O_3 of 1.93 [32] and the particle volume fraction of 0.596, one obtains the effective refractive index of 1.62, which was also derived from Yoldas mixing rule,[33] Bragg-Pippard,[34] Monecke,[35] and Fricke formulations.[36]

For a film of refractive index of 1.62 deposited on a fused silica substrate (1.46), the total single-pass Fresnel reflection loss at near-normal incidence does not exceed 10 %. The residual porosity is, thus, responsible for the decrease in transmittance around the wavelength of 612 nm by approximately 20 % in the absolute figures (i.e., the rest of the total transmission loss of 29 %). For shorter wavelengths, this contribution slowly increases reaching 40 % at the blue edge of the visible range (380 nm).

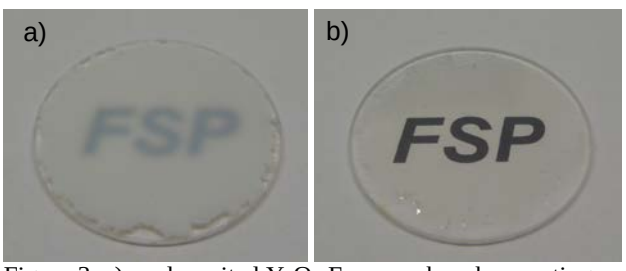

Figure 3. a) as-deposited Y_2O_3:Eu nanophosphor coating; b) compacted coating, 3.8 mg cm^{-2}.

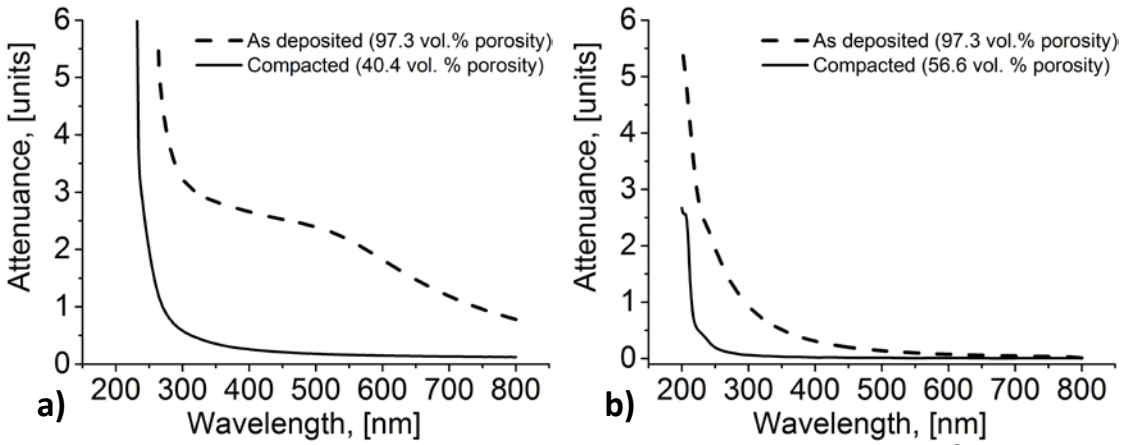

Figure 4. Attenuance of Y_2O_3:Eu nanophosphor coatings before and after compaction: a) 3.8 mg cm^{-2}; b) 0.23 mg cm^{-2}.

Figure 4b shows the evolution of attenuance of the thinnest compacted nanophosphor film. In the original state, transmittance decreased from 93 % around the wavelength of 800 nm to 42 % at 380 nm. In the same range, transparency of the compacted film only changed from 98.5 % to 94 % over the same wavelength range.

The decrease of scatterance, despite the fact that the number of nanoparticles each photon should intersect stays constant, should be attributed to the effects of dependent scattering. When the distance between the scattering centers falls short of the wavelength of the incident light, the scattering efficiency of each single particle starts to decrease. For nanoparticles with the size substantially below the wavelengths of visible light, the conditions for the onset of dependent scattering are fulfilled for any realistic packing density in the packed state.[19] Decreasing porosity is expected to reduce scattering. At the same time, absorption of light, which dominates the attenuation in the UV-range, should be much less affected by compaction. These predictions are supported by the experimental results in Figure 4.

Photoluminescent properties of the compacted nanophosphor coatings

Densification of nanophosphor films did not introd

uce any significant changes in the spectra of excitation and emission of luminescence (Figure 5). The main peak of emission was found at the wavelength of 612 nm – characteristic for Eu^{3+}-ions in cubic Y_2O_3. The excitation spectrum featured a wide peak in the range between 220 and 270 nm due to the charge transfer band (electrons from the valence band undergo transitions to the excited states of Eu-ions). At wavelengths shorter than 220 nm, fundamental absorption across the bandgap of yttrium oxide mainly contributes to excitation of photoluminescence.[37,38]

The main performance parameter of a luminescent material is the efficiency of conversion of the excitation energy in the emitted light. In the case of photoluminescence, it is described by a number ratio of emitted and absorbed photons usually termed *quantum yield* (QY). Under constant excitation conditions, QY is directly proportional to the intensity of emission so that an estimate of efficiency of a phosphor can be obtained by comparing its brightness with that of a sample with a known QY. Provided that the spectral distribution of emission is the same for both the material under investigation and the reference phosphor, it is sufficient to relate the intensities of the main emission peak.

In our previous work, from the typical quantum efficiency of commercial Y_2O_3:Eu phosphors (0.95)[39] and relative maximum brightness of the uncompacted Y_2O_3:Eu FAD-deposits (33 %),[11] an estimate of their quantum efficiency on the order of 0.31 could be obtained. Correcting this figure for up to 18 wt.% of "passively" absorbing monoclinic yttria present in the deposited films, the actual quantum efficiency of pure cubic

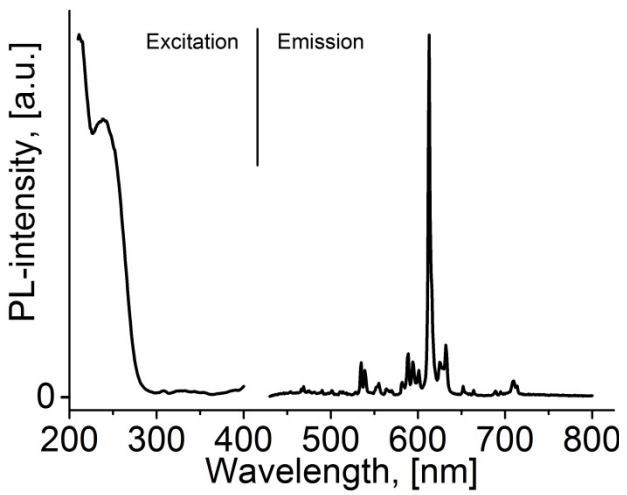

Figure 5. Spectra of excitation and emission of photoluminescence of the compacted FAD-deposited Y_2O_3:Eu nanophosphor coating.

phosphor phase should be approximately 0.38. Strictly speaking, the UV-light absorbed by the monoclinic phase is not completely lost as it also emits photoluminescence at different wavelengths. Nonetheless, this modification is substantially less efficient than the cubic one[11] and it does not any peaks of emission at 612 nm so that it is rejected in the measurements of brightness.

The changes of external QY after compaction featured a pronounced systematic dependence on the thickness of the films. The most prominent increase of the luminescence intensity measured normally to the surface of the substrate was observed for the thickest coatings (3.8 mg cm^{-2}) and was equal to 28 %. In this way, they reached 40 % of the maximum brightness of the coatings made of the commercial micrometer-sized Y_2O_3:Eu powder. At the same time, for the thinner coatings the PL-intensity emitted normal to the substrate usually even decreased, e.g., it dropped by 30 % for the coatings of 1.2 mg cm^{-2}, which possessed the highest brightness in the uncompacted state. In the case of the thinnest studied coating (0.23 mg cm^{-2}), the decrease of brightness was even more significant - nearly 60 %. Such a dependence of brightness on thickness of the nanophosphor films cannot be explained by variation of nanoparticle packing density/effective refractive index of the coatings and must be a result of a special loss mechanism.

Various sources of losses in the luminescent coatings were recently treated by G. Dantelle et al.[40] It was shown that in the absence of scattering in the phosphor film its brightness is severely affected by the light extraction issues. Light emitted in the volume of the phosphor coating experiences internal reflection at the interface with air. For the effective refractive index of 1.62, theoretically less than 11 % of the total emission intensity escapes at each of the two surfaces of the film; the rest 78 % (= 100 % – 11 % * 2) is trapped inside and experiences multiple internal reflections toward the edges of the sample. In the full absence of scattering, light trapping can cause the brightness drop by a factor of about 4.7. For the coatings investigated in this work, the 'guiding' effect is counteracted by the volume scattering due to residual porosity which, at least in the case of the thickest coatings, allows more than theoretically predicted 11 % of emission to escape from each surface of the film.

In the presence of light trapping processes, which are not active in uncompacted nanophosphor films or reference samples made from the strongly scattering commercial Y_2O_3:Eu powder, the direct comparison of PL-brightness cannot be reliably used for assessing QY of compacted samples. Alternatively, QY can be derived from the transient characteristics of emission[41]

$$QY = \frac{\tau}{\tau_R}, \qquad (2)$$

where τ and τ_R are the overall and the radiative exponential decay time constants, respectively. The experimentally observed overall emission decay time constant τ comprises contributions from radiative and non-radiative decay paths (τ_R and τ_{NR}, respectively)[41]

$$\frac{1}{\tau} = \frac{1}{\tau_R} + \frac{1}{\tau_{NR}}. \qquad (3)$$

Equations 2 and 3 can be combined. The experimentally observed decay time constant of emission changed from 3.27 to 1.40 ms, i.e., by a factor of 2.33 If the non-radiative decay time constant was assumed unaffected by compaction and the initial value of QY was 0.38, the absolute quantum efficiency of the cubic Y_2O_3:Eu nanopowder would have to increase by almost 100 % upon compaction to 59.6 vol.% and reach 0.73. The apparent efficiency of the nanophosphor with admixture of monoclinic phase should be then equal to 0.60 (i.e., 63 % of the maximum brightness of the coarse-grained commercial Y_2O_3:Eu reference). As anticipated from the lower particle volume fraction of the thinnest compacted coatings (43.4 vol.%), the corresponding luminescence decay time constant was longer than that of the thickest coatings (1.62 vs. 1.40 ms, respectively), which results in an estimate of the true quantum efficiency for the cubic phase of 0.69 and apparent efficiency of 0.57, thus still promising a drastic increase of QY.

The above estimates show that suppression of the light trapping in the compacted nanophosphor films would allow almost doubling the intensity of emission as compared to the initial, uncompacted state. Although the bright emission from the lateral edges of the samples could be observed visually, quantitative measurements of the total emission intensity could not be performed due to the lacking equipment. Therefore, another way to demonstrate the actual gain in QY of the nanophosphor films had to be found.

Introduction of a strongly scattering surface layer

One of the 1.2 mg cm^{-2} samples, which usually demonstrated a 30 % intensity drop upon compaction, was sandwiched not with a blank substrate but with a layer of strongly scattering submicrometer-sized particles of another phosphor, yttrium aluminum garnet (YAG) doped with terbium, produced by flame-assisted spray pyrolysis in our previous work.[42] YAG host is transparent down to a wavelength of 200 nm,[43] and photoluminescence of Tb-ion in YAG is not efficiently excited at 254 nm.[42] Compression by the otherwise standard CIP-assisted procedure resulted in a structure shown in Figure 6. The top surface of the nanophosphor film was covered with a rough particulate crust able to disrupt the multiple internal reflection of light. At the same time, full loss of transparency was observed (attenuace at the emission wavelength reached 1.9 units, i.e. less than 1.3 % transmittance, spectra not shown). In this experiment, the improvement of light extraction factor comes at cost of inferior transparency. However, it is not suggested as a general way of using the nanophosphor coatings but only intends to prove that the quantum efficiency indeed increases after compaction, while internal reflection of light is responsible for the losses of emission intensity in the thin films. Brightness of emission was measured in two configurations depicted

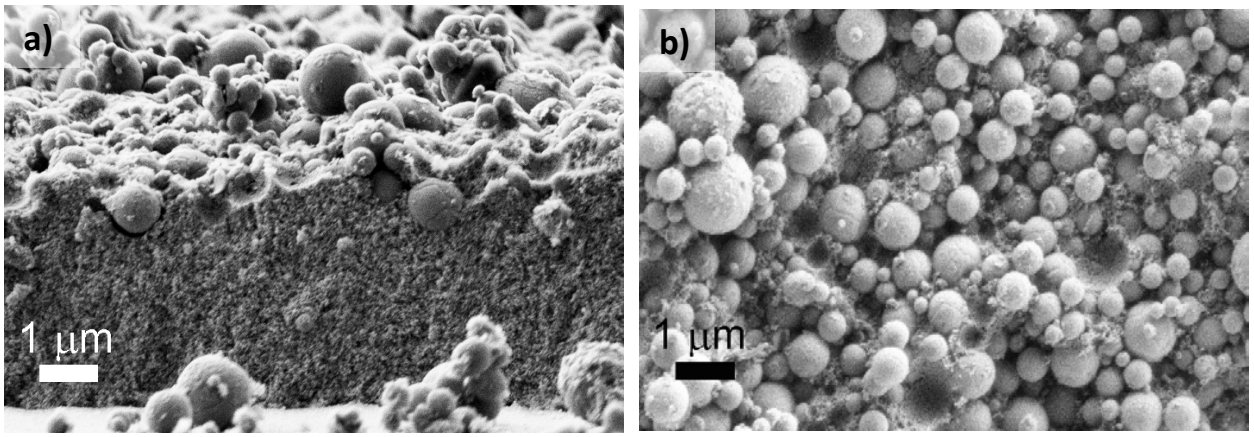

Figure 6. SEM-images of the Y_2O_3:Eu nanophosphor film covered with the YAG:Tb scatterers: cross-sectional view (a), top view (b).

in Figure 7 and referred to as forward (F) and backward (B) modes.

In the forward direction, the exciting radiation from the UV-lamp is first incident on the layer of scatterers, where a relatively large fraction of UV-light is diffusely reflected back from the sample (attenuance at 254 nm was reaching 2.6 units). UV-photons diffusely transmitted through the layer of YAG:Tb excite luminescence in the compacted Y_2O_3:Eu film. In spite of the fact that the flux of UV-photons reaching the Y_2O_3:Eu was diminished by scattering on YAG:Tb particles, PL-brightness of the sample in the conventional F-mode increased to 40 % of the commercial Y_2O_3:Eu phosphor, i.e. increased by at least 30 % of the initial value instead of the usually observed decrease.

By exposing the same sample to the UV-light in the backward direction, the loss of intensity of exciting UV-radiation by scattering on YAG:Tb particles could be avoided. Strong light scattering in this layer still could have a negative influence on measured PL-brightness as light generated in the nanophosphor film was diffusely reflected back to the substrate and could tend to preferably escape from the sample towards the UV-lamp and not towards the detector. Nevertheless, the brightness in the B-mode further increased and reached 55 % of the commercial coarse-grained reference, thus improving over the performance of the uncompacted nanophosphor film of the same coating density by nearly 70 %. Only weak traces of emission from YAG:Tb could be detected in both F- and B-configurations, which did not affect the measured values of brightness of compacted Y_2O_3:Eu nanophosphor as the contributions from both phosphors were spectrally resolved. It also has to be noticed that for the standard compacted Y_2O_3:Eu nanophosphor layers without deliberately introduced scatterers there was no significant difference between the PL-brightness obtained in the F- and B-modes.

Optimization of properties of the scattering layer potentially could allow further increasing of film brightness. From this point of view, it seems feasible to double the brightness of emission and approach the apparent quantum efficiency of 0.60 calculated above from the measured decay time constants and the initial quantum efficiency of 0.31.

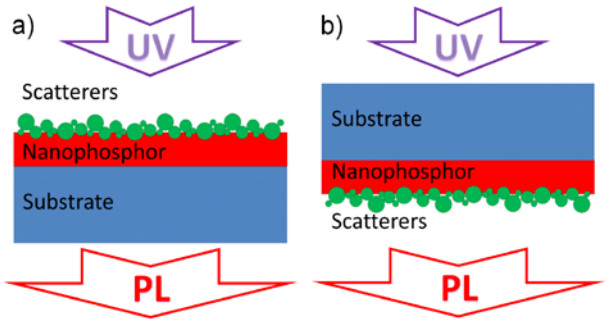

Figure 7. Configurations of a) forward (F-mode) and b) backward (B-mode) exposure of the sample containing scatterers.

Modeling of the photonic effects of compaction on the radiative decay rate of photoluminescence

The above estimates of boosted QY were obtained without making any explicit assumptions on the changes of the radiative decay rate. At the same time, the dependence of PL-performance on packing density of nanoparticles is mostly related to the shortening of the radiative decay time constant of excited ions embedded in media with higher refractive index. This relation is usually discussed in terms of two alternative approaches: a real cavity model and a virtual cavity model.[44,45] It has to be mentioned that these models are usually tested for luminescent centres dispersed in continuous liquids or solids of varying refractive index. To the best of our knowledge, the influence of compaction of nanophosphors not embedded in any dense media has not been reported.

The real cavity model assumes a substitutional impurity in an empty cavity having a refractive index of vacuum. The radiative decay time constant is expressed by[45]

$$\tau_R = \frac{1}{f(ED)} \frac{\lambda_0^2}{\left[\frac{3n_{EFF}^2}{2n_{EFF}^2+1}\right]^2 n_{EFF}}, \qquad (4)$$

where f(ED) is the oscillator strength of the specific electric dipole transition and λ_0 is the wavelength in vacuum. For the change of the effective refractive index from 1.02 to 1.62, it predicts shortening of τ_R by a factor of 2.5. Considering that at the same time the overall decay time constant changed by the factor of 2.33, the QY (Equation 2) and the maximum brightness of the nanophosphor films could improve by not more than approximately 5 %. Thus, it should be concluded that the real cavity model is inappropriate for the compacted nanophosphor coatings, although it was applied in majority of reports on embedding of emitting ions in media with different refractive indices.[45,46]

According to the virtual spherical cavity model, which assumes an interstitial impurity in a cavity with the refractive index of the surrounding medium, the change of the radiative decay constant can be expressed by the following equation[44,47]

$$\tau_R = \frac{1}{f(ED)} \frac{\lambda_0^2}{\left[\frac{1}{3}\left(n_{EFF}^2+2\right)\right]^2 n_{EFF}}. \qquad (5)$$

The increase of the effective refractive index of the coating from 1.02 to a value of 1.62 would result in shortening of the radiative decay time of the transition τ_R by a factor of 3.7 in this case.

For comparison, taking the overall decay time constant of 1.40 ms and the quantum efficiency of 0.73 for the pure cubic Y_2O_3:Eu in the compacted state, as it was calculated in the previous section, the radiative decay time constant must be equal to 1.92 ms. Thus, it would have decreased by a factor of 4.5 from the initial state (QY = 0.38, τ = 3.27 ms, τ_R = 8.65 ms).

If the virtual cavity model was used to predict the shortening of the radiative decay time constant (while leaving the initial QY unfixed), the values of 0.50 and 0.79 would be derived from Equations 2 and 3 for the initial and final quantum efficiencies of the thickest compacted nanophosphor coating, respectively. However, such high initial QY could not be confirmed by measurements of brightness. Additionally, the increase of QY upon compaction of investigated Y_2O_3:Eu nanophosphor appears limited to 58 %, which falls short of 70 % gain in brightness experimentally demonstrated in the previous section. Both contradictions could be resolved if the effective refractive index of the compacted nanophosphor was higher than 1.62. For example, the shortening of the radiative decay time constant by the factor of 4.5 would be expected for the refractive index of 1.73 corresponding to the particle volume fraction of 73 % by Equation 1. However, this result does not comply with the situation reflected in the SEM images. Achieving such a high packing density of ceramic nanoparticles for pressing with pressures below 1 GPa is also not expected from the literature on compaction of nanopowders.[48]

The inconsistency of experimental results for the decay of photoluminescence from rare earth-doped nanoparticles with either of the two discussed models was recognized by several researchers.[49,50] It was suggested that PL-properties of nanophosphors in media with different refractive indices can be better described by a modified empty cavity model, referred to as a nanocrystal cavity model, where the refractive index of vacuum is substituted for that of the host material of nanoparticles n_{NC}

$$\tau_R = \frac{1}{f(ED)} \frac{\lambda_0^2}{\left[\frac{3n_{EFF}^2}{2n_{EFF}^2+n_{NC}^2}\right]^2 n_{EFF}}. \qquad (6)$$

In this model, the radiative decay time constant decreases by a factor of 4.2 while n_{EFF} changes from 1.02 to 1.62. This value is very close to 4.5 calculated from the initial brightness of the coatings and measured decay time constants before and after compaction. Obviously, the nanocrystal cavity model is the most suitable for the nanophosphor coatings under investigation. The small residual difference could be attributed to either not precisely known refractive index of the phosphor material or underestimated initial QY of the coatings.

The relation between porosity and the effective refractive index of solid films is a subject of numerous studies[51,52] and there is no common opinion on which mixing rule is the most appropriate. It is known that experimentally measured values of the mean refractive index can exceed the estimates produced by approaches based on linear permittivity mixing,[53] such as the one applied here (see Equation 1). The effective refractive index could also be affected by the presence of monoclinic phase, which has higher gravimetric density and potentially should have somewhat higher refractive index. Unfortunately, no data on its value could be found in the literature so that its influence on the effective index of the studied films remains uncertain. No significant influence of Eu-doping on the average refractive index is expected as the refractive index of pure Eu_2O_3 (1.97)[32] is only slightly higher than that of Y_2O_3, and its concentration is relatively low.

As the value of the effective refractive index could not be exactly adjusted, the shortening of the radiative decay time constant by the factor of 4.2 can be used in further analysis as the worst-case scenario. According to Equation 2 and 3, an increase of QY of the pure cubic Y_2O_3:Eu to approximately 0.75 can be predicted for the compaction to 60 vol.%. In the absence of light trapping and assuming the presence of 18 wt.% of the "passive" monoclinic phase, the PL-brightness of the compact-

ed coating could ultimately reach 67 % of that of the state-of-the-art commercial coarse-grained reference.

By extrapolation of the dependence of QY of the cubic Y_2O_3:Eu nanophosphor for the case when the particle volume fraction equals 1.00 (pore-free solid), a value of 0.82 is obtained, i.e., 86 % of brightness of the benchmark commercial phosphor. The missing 14 % can be attributed to quenching on the surface or other defects of crystalline structure often observed for phosphor nanoparticles.[41,54] This also means that if further mechanical compaction was possible, it could not bring more than 10 % improvement over the QY of 0.75 already achieved in this study. It can be concluded that the investigated technique of cold compaction allows to appreciably narrow the gap in performance of nanophosphors and their micrometer-sized counterparts.

One can anticipate that obtaining the phase-pure cubic nanophosphor, suppression of "surface quenching" and light trapping would be more advantageous than the attempts to compact the films with even higher pressures. The pure cubic nanophosphor with the particle volume fraction of 60 % potentially could reach QY of 0.93 once the "surface quenching" is fully eliminated. The feasibility of reduction of negative effects of imperfect crystallinity and surface quenching on phosphor efficiency was already reported for several luminescencent nanopowders.[40,54]

Conclusions

Cold compaction of nanophosphor films deposited by flame aerosol deposition was shown to be a viable means to obtain optically transparent and mechanically stable coatings. Uniaxial compression between two rigid flat substrates pressurized isostatically by a conventional cold isostatic pressing can increase the packing density of phosphor nanoparticles from 2.7 vol.% to 59.6 vol.% without introducing cracks in the films. Hardness and elastic modulus of the compacted films reached 1.5 and 50 GPa, respectively, enabling safe handling and appreciable stability for demanding applications. Brightness of the films increased only slightly upon compaction or even decreased. From the decrease of the luminescence decay time constants, the increase of the apparent QY of nanophopshor from approximately 31 % to 60 % could be estimated. It was also possible to increase the light extraction efficiency from the compacted nanophosphor film by intentional introduction of a strongly scattering surface layer. The maximum brightness of the Y_2O_3:Eu nanophosphor coating of 1.2 mg cm^{-2} covered with a layer of sub-micrometer-sized YAG:Tb particles demonstrated the increase from 33 % to 55 % of brightness of the reference coarse-grained commercial phosphor powder coating, thus confirming a considerable increase in quantum yield of the nanophosphor.

Our data shows that the nanocrystal cavity model is the most appropriate for describing the variation of the radiative decay rate while neither the real nor virtual cavity models could be supported. Based on the chosen model, it is predicted that the further improvement of PL-performance can be rather achieved by synthesis of phase-pure nanophosphor and inhibition of "surface quenching" while compaction with even higher pressures would have only a minor effect.

Combination of FAD with CIP enables rapid deposition of optical coatings, starting from liquid precursors and ending with solid transparent films, within just several minutes and without exposing the substrates to very high temperatures (FAD on polymer substrates was already demonstrated).[17,18] By varying the applied pressure, it should be possible to tune the density, effective refractive index and transparency of the coatings. Multiple deposition and compression cycles with stepwise decreasing pressure could facilitate fabrication of structures with graded refractive index to counteract the effect of light trapping while sustaining optical transparency of the structures.[55]

CIP-assisted cold compaction can be applied to any other nanoparticulate films, including other phosphor materials, flexible substrates, and coatings deposited by methods other than flame spray pyrolysis. Nanoparticulate coatings compacted by the suggested technique can also be used for producing polymer-infiltrated composites[18] with ultra-high nanoparticle loading comparable to those produced, for example, by a recently published Capillary Rise Infiltration method.[56]

Acknowledgements

The authors gratefully acknowledge technical assistance of K. Fujiwara and C. O. Blattmann (ETH Zurich), M. Ritter and P. N. Dyachenko (TUHH). We also thank A. Yu. Petrov (TUHH) for fruitful discussions and S. E. Pratsinis (ETH Zurich) for support and comments on the manuscript. The work was financially supported by the German Research Foundation (DFG) via SFB 986 "Tailor-Made Multi-Scale Materials Systems: M^3", projects A6, C2, and C4.

Notes and references

[a] Institute of Advanced Ceramics, Hamburg University of Technology (TUHH), Denickestrasse 15, 21073 Hamburg, Germany.

[b] Current address: Laboratory for High Performance Ceramics, Swiss Federal Laboratories for Materials Science and Technology (EMPA), Überlandstrasse 129, 8600 Dübendorf, Switzerland.

1 W.-S. Song, K.-H. Lee, Y. R. Do and H. Yang, *Adv. Funct. Mater*. 2012, **22**, 1885–1893.

2 R. Kasuya, A. Kawano, T. Isobe, H. Kuma and J. Katano, *Appl. Phys. Lett.* 2007, **91**, 111916.

3 X. Huang, S. Han, W. Huang and X. Liu, *Chem. Soc. Rev.* **2013**, *42*, 173–201.

4 C. Lin, M. T. Berry, R. Anderson, S. Smith and P. S. May, *Chem. Mater*. 2009, **21**, 3406–3413.

5 Y. Peng, J. Liu, K. Zhang, H. Luo, J. Li, B. Xu, L. Han, X. Li and X. Yu, *Appl. Phys. Lett.* 2011, 99, 121110.

6 A. Revaux, G. Dantelle, D. Decanini, A.-M. Haghiri-Gosnet, T. Gacoin and J.-P. Boilot, *Opt. Mater.* 2011, **33**, 1124–1127.

7 B. Fleury, G. Dantelle, S. Darbe, J. P. Boilot and T. Gacoin, *Langmuir* 2012, **28**, 7639–7645.

8 S. Watanabe, T. Asanuma, H. Hyodo, K. Soga and M. Matsumoto, *Langmuir* 2013, **29**, 11185–11191.
9 S. Watanabe, Y. Hamada, H. Hyodo, K. Soga and M. Matsumoto, *J. Colloid Interface Sci*. 2014, **422**, 58–64.
10 Y. Iso, S. Takeshita and T. Isobe, *Langmuir* 2014, **30**, 1465–1471.
11 R. Kubrin, A. Tricoli, A. Camenzind, S. E. Pratsinis and W. Bauhofer, *Nanotechnology* 2010, **21**, 225603.
12 L. Mädler, H. Kammler, R. Müller and S.E. Pratsinis, *J. Aerosol Sci.* 2002, **33**, 369-389.
13 A. Mendez and T. F. Morse, *Specialty optical fibers handbook*, Elsevier/Academic Press, Amsterdam 2007.
14 L. Mädler, A. Roessler, S. E. Pratsinis, T. Sahm, A. Gurlo, N. Barsan and U. Weimar, *Sens. Actuator. B* 2006, **114**, 283–295.
15 A. Tricoli, M. Righettoni and S. E. Pratsinis, *Langmuir* 2009, **25**, 2578–12584.
16 A. Tricoli, A. S. Wallerand and M. Righettoni, *J. Mater. Chem.* 2012, **22**, 14254–14261.
17 T. Rudin, K. Tsougeni, E. Gogolides and S. E. Pratsinis, *Microelectron. Eng.* 2012, **97**, 341–344.
18 G. A. Sotiriou, C. O. Blattmann and S. E. Pratsinis, *Adv. Funct. Mater.* 2013, **23**, 34–41.
19 R. Kubrin, *KONA Powd. Part. J*. 2014, **31**, 22-52.
20 H. Lindström, A. Holmberg, E. Magnusson, S.-E. Lindquist, L. Malmqvist and A. Hagfeldt, *Nano Lett.* 2001, **1**, 97–100.
21 G. Boschloo, H. Lindström, E. Magnusson, A. Holmberg and A. Hagfeldt, *J. Photochem. Photobiol. A* 2002, **148**, 11-15.
22 M. Durr, A. Schmid, M. Obermaier, S. Rosselli, A. Yasuda and G. Nelles, *Nature Mater.* 2005, **4**, 607-611.
23 J. Halme, J. Saarinen and P. Lund, *Sol. Energy Mater. Sol. Cells* 2006, **90**, 887-899.
24 T. Yamaguchi, N. Tobe, D. Matsumoto and H. Arakawa, *Chem. Commun.* 2007, 4767-4769.
25 S. O. Schopf, S. Salameh and L. Mädler, *Nanoscale* 2013, **5**, 3764-3772.
26 Y. Peng, J. Z. Liu, K. Wang and Y.-B. Cheng, *Int. J. Photoenergy* 2011, **2011**, 410352.
27 H. C. Weerasinghe, P. M. Sirimanne, G. P. Simon and Y.-B. Cheng, *J. Photochem. Photobiol. A* 2009, **206**, 64-70.
28 H. C. Weerasinghe, P. M. Sirimanne, G. P. Simon and Y.-B. Cheng, *Prog. Photovolt. Res. Appl.* 2012, **20**, 321-332.
29 R.Kubrin, W. Bauhofer and A. Ivankov, *J. Electrochem. Soc.* **2007**, *154*, J253-J261.
30 M. N. Rahaman, *Ceramic processing*, CRC/Taylor & Francis, Boca Raton, FL, USA 2007.
31 I. C. Albayrak, S. Basu, A. Sakulich, O. Yeheskel and M. W. Barsoum, *J. Amer. Ceram. Soc.* 2010, **93**, 2028-2034.
32 R. D. Shannon, R. C. Shannon, O. Medenbach and R. X. Fischer, *J. Phys. Chem. Ref. Data* 2002, **31**, 931-970.
33 B. E. Yoldas, *Appl. Opt.*, 1980, **19**, 1425-1429.
34 W. L. Bragg and A. B. Pippard, *Acta Crystallogr.*, 1953, **6**, 865-867.
35 J. Monecke, *J. Phys. Cond. Matter*, 1994, **6**, 907-912.
36 M. Kobayashi and H. Terui, *Appl. Opt.*, 1983, **22**, 3121-3127.
37 G. Blasse and B. C. Grabmaier, *Luminescent materials*, Springer, Berlin, etc., 1994.
38 L. Ozawa, *Cathodoluminescence and photoluminescence. Theories and practical applications*, CRC Press, Boca Raton, Fla., USA 2007.
39 A. H. Kitai, *Solid state luminescence. Theory, materials and devices*, Chapman & Hall, London 1993.
40 G. Dantelle, B. Fleury, J.-P. Boilot and T. Gacoin, *ACS Appl. Mater. Interfaces* 2013, **5**, 11315-11320.
41 C. Ronda, *Luminescence. From theory to applications*, Wiley-VCH, Weinheim 2008.
42 R. Kubrin and W. Bauhofer, *Mater. Sci. Eng. B* 2012, **177**, 1605-1611.
43 G. A. Slack, D. W. Oliver, R. M. Chrenko and S. Roberts, *Phys. Rev.* 1969, **177**, 1308-1314.
44 R. S. Meltzer, S. P. Feofilov, B. Tissue and H. B. Yuan, *Phys. Rev. B* 1999, **60**, R14012.
45 K. Dolgaleva, R. W. Boyd and P. W. Milonni, *J. Opt. Soc. Am. B*, 2007, **24**, 516-521.
46 F. J. P. Schuurmans, D. T. N. de Lang, G. H. Wegdam, R. Sprik and A. Lagendijk, *Phys. Rev. Lett.*, 1998, **80**, 5077-5080.
47 B. Henderson and G. F. Imbusch, *Optical spectroscopy of inorganic solids*, Clarendon Press, Oxford, 1989.
48 K. Lu, *Nanoparticulate materials. Synthesis, characterization, and processing*, John Wiley & Sons, Hoboken, NJ, USA 2013.
49 C.-K. Duan and M. F. Reid, *J. Alloys Comp.* 2006, **418**, 213-216.
50 T. Senden, F. T. Rabouw, A. Meijerink, *ACS Nano* 2015, in press, DOI: 10.1021/nn506715t.
51 N. K. Sahoo, S. Thakur, R. B. Tokas and N. M. Kamble, *Appl. Surf. Sci.*, 2007, **253**, 6787-6799.
52 E. V. Astrova and V. A. Tolmachev, *Mater. Sci. Eng. B*, 2000, **69-70**, 142-148.
53 Y. Tamar, M. Tzabari, C. Haspel and Y. Sasson, *Sol. Energy Mater. Sol. Cells* 2014, **130**, 246–256.
54 I. Maurin , G. Dantelle , J.-P. Boilot and T. Gacoin, *J. Mater. Chem. C* 2013, **1**, 13-22.
55 F. W. Mont, J. K. Kim, M. F. Schubert, E. F. Schubert and R. W. Siegel, *J. Appl. Phys.* 2008, **103**, 083120.
56 Y. Huang, Y. Jiang, J. L. Hor, R. Gupta, L. Zhang, K. J. Stebe, G. Feng, K. Turner and D. Lee, *Nanoscale* 2015, **7**, 798-805.

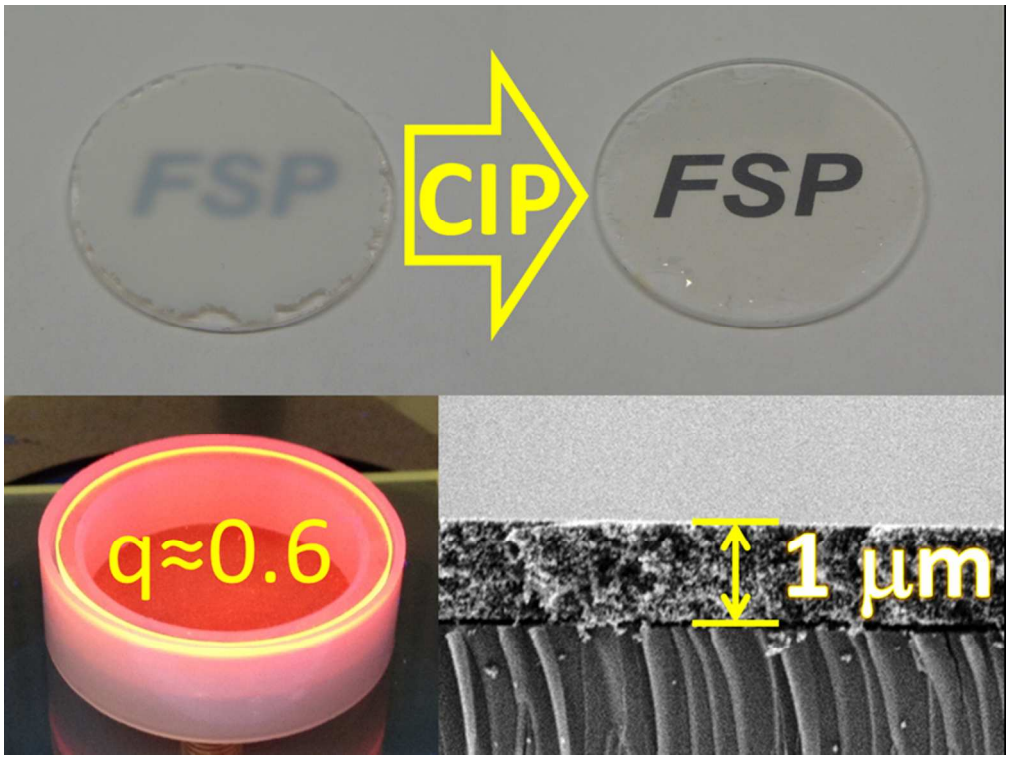

158x118mm (150 x 150 DPI)